Elevate Series

ALL EARTH
2026, VOL. 38, NO. 1, 2711157
https://doi.org/10.1080/27669645.2026.2711157

RESEARCH ARTICLE

Evolutionary and ecological correlates of avian uncinate process morphology: insight from a bizarre shape found in Early Cretaceous Enantiornithes

Pei-Chen Kuo[a,b], Yan Wang[c,d], Alexander D. Clark[b,e], Corwin Sullivan[f,g], Xiaoli Wang[c,d], Xiaoting Zheng[d] and Jingmai K. O'Connor[b]

[a]Key Laboratory of Vertebrate Evolution and Human Origins, Institute of Vertebrate Paleontology and Paleoanthropology, Chinese Academy of Sciences, Beijing, China; [b]Negaunee Integrative Research Center, Field Museum of Natural History, Chicago, IL, USA; [c]School of Life Sciences, Linyi University, Linyi, Shandong, China; [d]Tianyu Natural History Museum of Shandong, Pingyi, Shandong, China; [e]Committee on Evolutionary Biology, University of Chicago, Chicago, IL, USA; [f]Department of Biological Sciences, University of Alberta, Edmonton, Canada; [g]Philip J. Currie Dinosaur Museum, Wembley, Canada

ABSTRACT

The avian uncinate process, a bony projection of the thoracic ribs, has been linked to flight performance and physiology. Its morphology exhibits considerable shape variation, which is potentially driven by ecological factors. Here, we describe a new enantiornithine bird (specimen STM11-128) from the Lower Cretaceous Jehol Group with unusual uncinate processes and comprehensively compare shape variance of the uncinate process between Mesozoic stem avian clades and extant Neornithes. Using landmark-based geometric morphometric and phylogenetic comparative methods, we quantify morphological variation of the uncinate process and explore its relationship with key ecological features across a broad phylogenetic sampling. We found that shape variation of the uncinate process shows a weak association with the examined ecological categories. In contrast, uncinate process length shows a stronger association with several ecological attributes, suggesting that avian uncinate process length strongly influences its mechanical benefits, with little impact from its shape. Finally, when comparing morphological variation across different clades of non-neornithine Mesozoic birds and modern birds, Mesozoic avian uncinate processes are characterised by a slender profile, whereas the shape of neornithine uncinate processes shows significantly higher diversity. This at least partially reflects a sampling bias as these small processes are rarely preserved in fossils.

ARTICLE HISTORY
Received 8 January 2026
Accepted 24 July 2026

KEYWORDS
Aves; uncinate process; geometric morphometric analysis; Ecomorphology

1. Introduction

The respiratory system in birds is unique among vertebrates, consisting of a pair of lungs and a series of air sacs that are rigidly attached to and are contacted with the vertebral ribs, respectively (Codd, 2010; Lawson et al., 2021). During respiration, movements of the ribs, uncinate processes, and sternum, facilitated by the associated muscles, cause the air sacs to act like bellows, generating a one-way flow of air through the paleopulmo region of the lung (Bretz & Schmidt-Nielsen, 1972; Codd, 2010; Scheid & Piiper, 1972). The uncinate processes are dorsocaudally oriented bony projections extending off the caudal (posterior) cervical and/or cranial (anterior) thoracic (dorsal) ribs in most birds, although they are notably absent in anhimids (screamers) and megapodiids (megapodes) (Baumel, 1993). Evidence indicates these structures have deep roots in the evolutionary history of archosaurs but remained cartilaginous in all but derived maniraptoran theropods (Codd et al., 2008; Wang et al., 2023). Generally, five to six pairs of uncinate processes are present. These processes are narrow and elongate in most extant avian taxa (Figure 1(A)), and the first two processes are significantly shorter than the following ones (Fig. S9A). However, variation exists, with some taxa exhibiting distinct morphologies (e.g. Alagoas curassow [*Mitu mitu*], triangular (Figure 1(B)); Hoatzin [*Opisthocomus hoazin*], weakly developed (Figure 1(C)); Blue-and-yellow macaw [*Ara ararauna*], rectangular base (Figure 1(D))). In some species the shape of the uncinate processes changes along the series. In the

CONTACT Yan Wang wangyan6696@lyu.edu.cn School of Life Sciences, Linyi University, Linyi, Shandong 276005, China
Supplemental data for this article can be accessed online at https://doi.org/10.1080/27669645.2026.2711157.

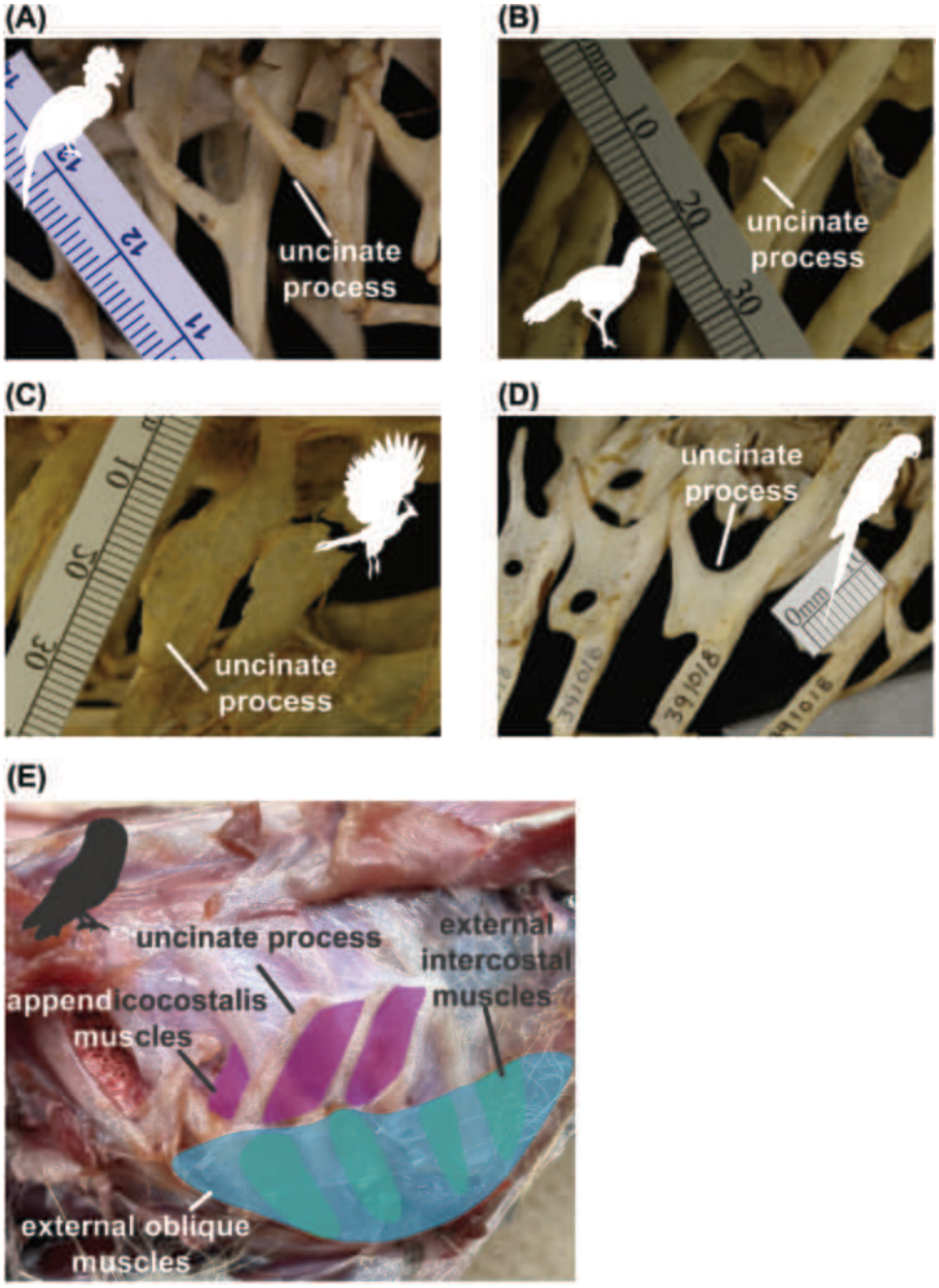

Figure 1. Morphologically diverse crown avian uncinate processes (A-D), and associated musculature (E). (A) Great blue turaco (*Corythaeola cristata*); (B) Alagoas curassow (*Mitu mitu*); (C) Hoatzin (*Opisthocomus hoazin*); (D) Blue-and-yellow macaw (*Ara ararauna*) (E) Dissected abdominal region of Barn owl (*Tyto alba*) in left lateral view. Silhouettes either (1) based on Prof. Daniel Field Flicker photos or (2) from PhyloPic.org.

Grey-winged trumpeter (Fig. S9B), for example, the first two and the last uncinate processes are slender, tapering rods while the third and fourth uncinate processes are L-shaped with a ventral expansion.

Movements of the uncinate processes are controlled by several important muscles related to locomotion and the respiratory system (e.g. external intercostal muscles for stabilisation of trunk, and appendicocostalis and external oblique muscles for respiration) (Codd et al., 2005). Each external intercostal muscle slip originates on the cranial margin of a rib and inserts on the caudal margin of the preceding rib (Figure 1 (E)). The appendicocostalis muscles originate on the cranial margin of the rib and insert on the caudal margin of the uncinate process of the preceding rib (Figure 1(E)). The external oblique muscle originates on the base of the sternal plate, down to the xiphoid process, and insert on the ventral margins of the proximal halves of

the uncinate processes (Figure 1(E)). Therefore, the shapes and lengths of the uncinate process potentially impact the functioning of these three muscles, which are strongly associated with the respiratory system.

The uncinate processes provide attachment surfaces for important muscles associated with locomotion and respiration (Codd et al., 2005), suggesting that the shape and length of the processes are likely driven by ecological factors. The presence of uncinate processes is hypothesised to increase the mechanical advantage (i.e. the ratio of output force to input force, an important aspect of muscle performance) of the muscles that attach to them (Kardong, 1988; Walker and Liem, 1994; Sereno, 1997; Liem et al., 2001). For example, uncinate processes can increase the mechanical advantage of the appendicocostalis muscles by a factor of 2–4, compared to the absence of these features (Tickle et al., 2007). It has been proposed that the uncinate processes may be linked to adaptations for different types of locomotion, such as flight and resting (Welty, 1988; Codd et al., 2005) since the external intercostal muscles are almost exclusively active during walking, whereas the appendicocostalis muscles are more active during sitting than during walking or standing (Codd et al., 2005). The elongated uncinate process also likely facilitate breathing through enhanced movements of the ribs and sternum (Tickle et al., 2009) as the uncinate processes also provide insertion surfaces for muscles associated with the respiratory system (i.e. appendicocostalis and external oblique muscles) (Codd et al., 2005).

Given the important role of uncinate processes in respiration and locomotion, variation in the shape of these bony projections may be associated with ecological factors (e.g. habitat, trophic level, trophic niche, primary lifestyle, or body mass) that vary widely across Aves. Because the uncinate processes serve as attachment sites for muscles involved in ventilation and flight performance, differences in their shape may influence muscle leverage, attachment area, or the mechanics of rib and sternal movements. Such morphological variation may therefore reflect differences in respiratory demands associated with body size and locomotion. Nevertheless, this morphological variation has received little attention, and the relationship between uncinate process shape and various ecological factors in extant birds have not been comprehensively examined. The evolutionary trajectory of uncinate process shape in birds has also not been significantly explored. The discovery of a new enantiornithine bird (STM11-128) from the Lower Cretaceous Jehol deposits with distinctly shaped uncinate processes provides a novel opportunity to assess the nature and potential ecological drivers of variation in these structures, and to investigate the evolutionary trajectory of uncinate process shape from extinct Mesozoic avians to extant neornithines. In this study, we quantified the variation in uncinate process across a broad sample of extant birds and examine its association with ecological factors using geometric morphometric analysis and phylogenetic comparative approach. Building on the relationship between uncinate process shape of extant birds, respiration, and locomotion, this study provides a framework for early avian respiratory function, and more generally on the role of uncinate processes in the early evolution of Mesozoic birds.

Abbreviations: DNHM: Dalian Natural History Museum, Dalian, Liaoning, China; IVPP: Institute of Vertebrate Palaeontology and Palaeoanthropology of the Chinese Academy of Sciences, Beijing, China; STM: Tianyu Museum of Nature, Pingyi, Shandong, China

2. Material & methods

2.1. Description of Enantiornithes sp. STM11-128

2.1.1. Location and formation

Lamadong Town, Jianchang County, Liaoning Province, China. Jiufotang Formation.

2.1.2. General description

The skeleton of STM11-128 is poorly preserved with the bones heavily crushed, but most skeletal elements are preserved *in situ*. (Figure 2(A,B)). The rostral portions of the skull and mandible are laterally exposed, while the caudal portions are exposed ventrally. However, it is impossible to confidently identify any palatal elements due to poor preservation. The dentaries are straight and elongate. Both the premaxillary and the dentary teeth are robust and triangular in profile, but teeth are restricted to the rostral portions of the upper and lower jaws.

Four postatlantal cervical vertebrae are exposed, indicating that there were at least five cervicals, but the neck was likely much longer (9–10 vertebrae) as in other enantiornithines. The fourth preserved cervical is the longest, while the third cervical is equal in length and width. Both preserve the neural spine, which forms a low

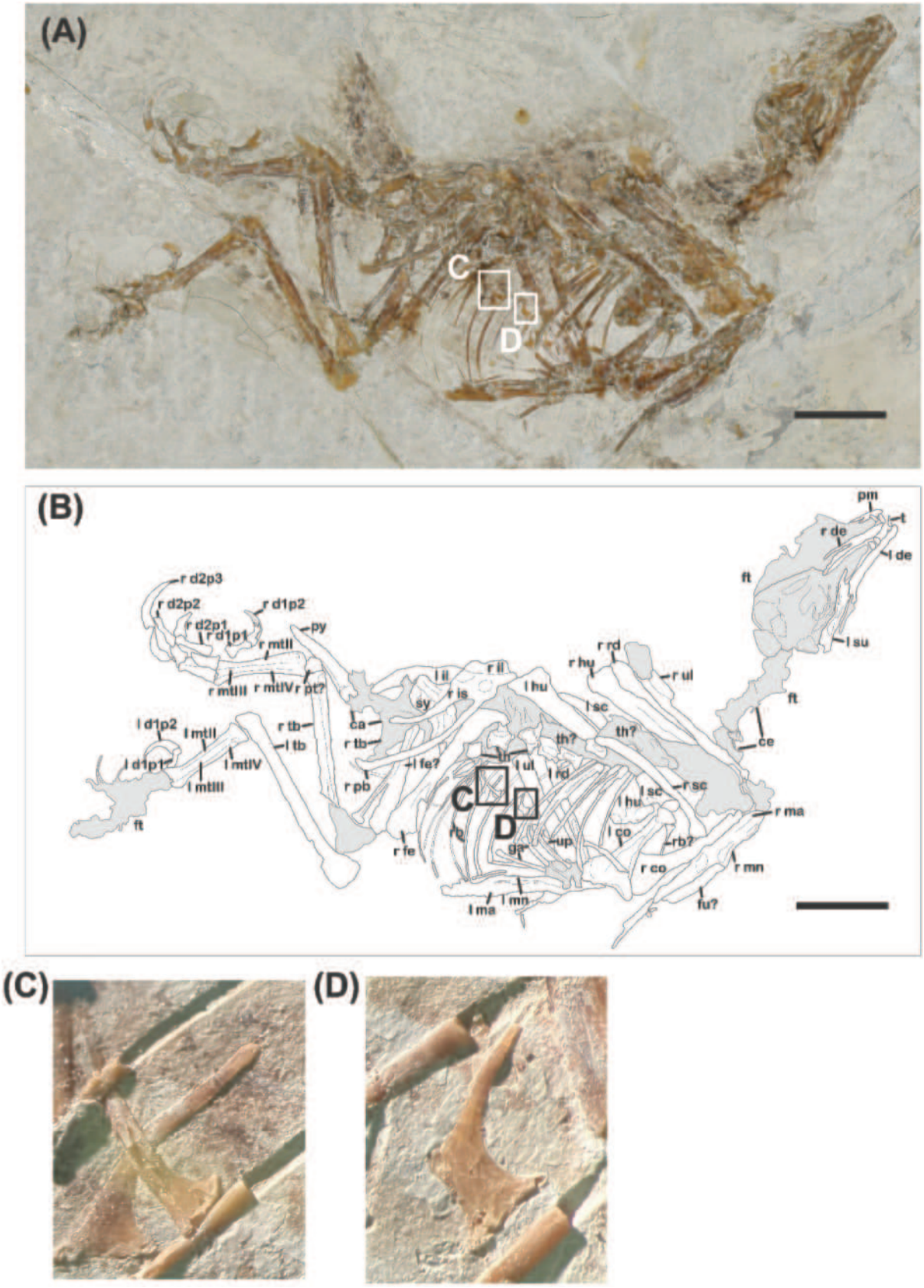

Figure 2. Enantiornithine STM 11–128. Photograph of the specimen (A), interpretive line drawing of the preserved elements (B), and photos showing the morphology of representative uncinate processes (C–D). Anatomical abbreviations: ca: caudal vertebrae; ce: cervical vertebrae; co: coracoid; d: digit; de: dentary; fe: femur; ft: fragment; fu: furcula; ga: gastralia; h: humerus; il: ilium; is: ischium; l: left; ma: major metacarpal; mn: minor metacarpal; mt I–IV: metatarsals I–IV; p: phalanx; pb: pubis; pm: premaxilla; py: pygostyle; pt: patella; r: right; rb: rib; rd: radius; sc: scapula; su: surangular; sy: synsacrum; t: teeth; tb: tibia; th: thoracic vertebrae; ul: ulnare; up: uncinate process. Scale bar for A–B: 20 mm. Light grey indicates areas of bone that are broken or poorly preserved.

midline crest. The prezygapophyses are much longer than the postzygapophyses. At least seven thoracic vertebrae are laterally exposed, revealing deeply excavated lateral fossae on their centra. At least three caudal vertebrae are articulated in sequence with the synsacrum, but they are partially covered by the right ischium, and two free caudal vertebrae are articulated in sequence with the pygostyle. The pygostyle of STM 11–128 shows the typical robust enantiornithine morphology with ventrolateral processes and a distally constricted tip (O'Connor, 2022), and is approximately equal to the tarsometatarsus in length. Fourteen dorsal ribs are preserved, indicating seven ribs for each side. Six uncinate processes are present and articulated with the 2nd to 5th ribs, without fusing to the ribs as in most extant birds. Approximately three pairs of sternal ribs are preserved, but unfortunately, the sternum itself is missing.

The coracoid is fan-shaped with a narrow neck and expanded pterygoma; a broad fossa is visible on the dorsal surface of the left coracoid. The medial side of the left coracoid is concave, and strongly curved where it begins to extend towards the *angulus medialis*, while the lateral margin is only weakly concave. The acromion process of the left scapula is square-shaped and robust. The humerus appears to be equal in length to the ulna and radius. The minor metacarpal is bowed and extends farther distally than the major metacarpal, as in other enantiornithines (Chiappe & Walker, 2002; O'Connor, 2022). The alular digit is short, ending just proximal to the distal margin of the major metacarpal. The right pelvis is fully articulated. The dorsal margin of the ilium expands caudodorsally, forming a blunt but robust crest. The pubis is elongate and much longer than the ischium. The ischium is dorsally concave and parallel to the retroverted pubis. The proximal end of the right tibia is blunt, with a flat articular surface. Metatarsal II is inwardly curved (the distal portion expands laterally). Metatarsal III is much longer than metatarsals II and IV. The first phalanx of right digit I (hallux) shows a distinct collateral ligament fossa. The digit I ungual is strongly curved; the other pedal claws are longer but less curved. STM11-128 was roughly the size of the extant Indian roller (*Coracias benghalensis*) (~171 g), estimated from humeral length using the equations presented by Field et al. (2013).

2.1.3. Description of the uncinate processes

Five uncinate processes are preserved in articulation or near-articulation with the 2nd to 5th dorsal ribs. The uncinate processes are not fused to the ribs, a condition consistent with observations from other non-ornithurine birds (Chiappe et al., 2020). The uncinate processes change slightly in shape from cranial to caudal. The uncinate process associated with 2nd and 3rd dorsal ribs are partially exposed. The uncinate process on the fourth rib is hook-like, with a rectangular base that forms a 100° angle with the tapering distal 2/3 such that the cranial margin is concave (Figure 2(D)). The tips of the two fourth-rib uncinate processes point dorsally, almost parallel to the ribs (~11°). The caudalmost uncinate processes, belonging to the fifth rib pair, have a simple shape with a fan-like base and a tip pointing caudodorsally (Figure 2(C)). In most enantiornithines, the uncinate processes have a simple rod-like appearance, and the hook-like morphology of most of the uncinate processes in STM11-128 is not accompanied by any other conspicuously unusual morphological features that might help to explain their atypical appearance.

2.2. Dataset, phylogenetic hypothesis and ecological information

We selected 136 extant avian species representing most neornithine clades, and seven Mesozoic birds, for our two-dimensional geometric morphometric analysis of uncinate process morphology. For extant avian species, following Tickle et al. (2009), we used photographs taken in the bird collections at the Field Museum (Chicago, IL, U.S.A.) and examined variation in the morphology of the uncinate process associated with the fourth vertebral rib. If the uncinate process of the fourth vertebral rib was not available in a particular specimen, that of the third rib was used instead. For Mesozoic birds, we sampled specimens from the Shandong Tianyu Museum of Nature (Shandong, China) and the literature (Chiappe et al., 2014; Clarke et al., 2006; Hu & O'Connor, 2017; Hu et al., 2015; O'Connor & Zhou, 2013; Zhou et al., 2014).

The foraging autecology of each species in our dataset was characterised using five ecological parameters: trophic level (discrete: herbivore, carnivore, scavenger), trophic niche (discrete: frugivore, granivore, nectarivore, terrestrial herbivore, aquatic herbivore, invertivore, vertivore, aquatic predator, scavenger), habitat (discrete: forest, woodland, riverine, grassland, wetland, shrubland, human modified, marine, coastal, rock), primary (foraging) lifestyle (discrete: aerial, insessorial, terrestrial, aquatic, generalist), and flight performance. Following Widrig et al. (2025); Kotnour et al. (2022) and Lowi-Merri et al. (2021), we recognised

eight flight performance (continuous flapping, flap-gliding, soaring, intermittent bounding, hovering, burst flight, powered swimming, flightless). Additional variables examined here were uncinate process size (continuous, quantified as log10-transformed centroid size, see below), uncinate process length (continuous, quantified as log10-transformed absolute length), uncinate process relative length (continuous, quantified as the ratio of log10-transformed absolute length and log10-transformed body mass, see below), body mass (continuous, quantified as log10-transformed body mass), phylogeny (discrete; Palaeognathae, Galloanserae, Strisores, Columbaves, Gruiformes, Aequorlitornithes, Inopinaves). The size of the uncinate process was estimated from the centroid size of landmark constellations from one of outputs of the 'gpagen' function of the *geomorph* 4.04 R package (Adams et al., 2022). Data on trophic level, trophic niche, habitat, primary lifestyle and body mass were retrieved from the global AVONET database (Tobias et al., 2022). For extinct birds, body mass was estimated from limb bone lengths (Field et al., 2013).

To explore the relationship between uncinate process morphology and autecologies, a phylogenetic generalised least-squares (PGLS) analysis was conducted for the extant bird dataset (n = 136). The time-calibrated phylogeny was constructed using a fossil-calibrated genome-level molecular analysis (Prum et al., 2015) and subclade-focused studies (Kimball et al., 2021; Kirchman et al., 2021; Lerner & Mindell, 2005; Liu et al., 2014; McGuire et al., 2014; Oliveros et al., 2019; Sorensen & Payne, 2005; Vianna et al., 2020). Our topology was built using Mesquite v. 3.61 (Maddison & Mddison, 2019), and the resulting phylogenetic tree was calibrated using *paleotree* v.3.4.4 (Bapst, 2012) within the R statistical environment v. 4.2.1 (R Core Team, 2022). Downstream analyses were also undertaken in the R statistical environment. The divergence time of major subclades was estimated from recent genome-level molecular analyses (Oliveros et al., 2019; Prum et al., 2015), and the ages of uncalibrated nodes were estimated using the 'timePaleoPhy' function of *paleotree* with the 'equal' time-scaling method.

In order to estimate the proportion of uncinate process length and morphological variation attributable to our selected ecological predictors, the 'varpart' function of the *vegan* v.2.6.-4 package (Oksanen et al., 2022) was applied. For the uncinate process length, we incorporated three ecological factors (body mass, trophic niche , and flight performance) into variance partitioning analyses due to the higher R^2 values (Table 1). For the morphological variation of uncinate process, three ecological attributes (body mass, habitat, and primary lifestyle) were selected based on the associated relationship in PGLS regression.

Table 1. Summary of the PGLS liner models for uncinate process length and relative length in Neornithes (n = 139) as a function of ecology information (body mass, primary habitat, trophic level, trophic niche, primary lifestyle, and flight performance), phylogenetic group, and its interaction.

ANOVA Syntax	λ	SS	MS	R^2	F	Z	P
Length~Body Mass	**0.9193368**	**0.143668**	**0.143668**	**0.79737**	**539.11**	**8.9179**	**1e-04**
Length~Habitat	**0.7937113**	**0.020345**	**0.0025431**	**0.13124**	**2.4548**	**2.1519**	**0.0165**
Length~Phy.group	0.7533949	0.013344	0.0022239	0.08874	2.1423	1.6347	0.0508
Length~ Trophic.Level	0.8507144	0.005519	0.0018396	0.0337	1.5694	0.86034	0.1984
Length~ Trophic.Niche	**0.7342858**	**0.032329**	**0.0035921**	**0.21772**	**3.9892**	**3.7422**	**1e-04**
Length~ Primary.Lifestyle	**0.8412184**	**0.018377**	**0.0045943**	**0.11338**	**4.2841**	**2.7814**	**0.002**
Length~ Flight.Performance	**0.6353263**	**0.044381**	**0.0063402**	**0.31433**	**8.579**	**5.4325**	**1e-04**
Length~Body Mass:Habitat	0.8838184	0.002210	0.000276	0.01296	1.1486	0.4143	0.3397
Length~Body Mass: Phy.group	**0.9778685**	**0.004379**	**0.000730**	**0.02118**	**2.6430**	**2.0491**	**0.0198**
Length~Body Mass: Trophic.Niche	0.9927692	0.002496	0.000312	0.01144	1.0483	0.2468	0.4038
Length~Body Mass: Primary.Lifestyle	0.8950404	0.000709	0.000177	0.00409	0.6652	−0.2870	0.6108
Length~Body Mass: Flight.Performance	0.8988029	0.001719	0.000246	0.00986	0.9215	0.0216	0.4942
Length~Habitat: Phy.group	0.7846932	0.015476	0.00085976	0.10056	0.8181	−0.46063	0.6793
Length~Habitat: Trophic.Niche	0.7881395	0.014343	0.00084370	0.09294	0.9371	−0.0760	0.5299
Length~Habitat: Primary.Lifestyle	0.8195396	0.011274	0.0007047	0.07108	0.7082	−0.80459	0.7878
Length~Habitat: Flight.Performance	0.7316441	0.009998	0.0005262	0.06745	0.6630	−1.0567	0.8538
Length~Phy.group: Trophic.Niche	0.7314491	0.018019	0.00120129	0.12157	1.3925	0.99287	0.1643
Length~Phy.group: Primary.Lifestyle	0.833089	0.010160	0.0011289	0.06321	1.0669	0.26745	0.3951
Length~Phy.group: Flight.Performance	0.5452874	0.005267	0.0006584	0.03841	0.9363	0.0303	0.4854
Length~ Trophic.Niche: Primary.Lifestyle	0.7713945	0.013090	0.00093497	0.08593	1.0617	0.25423	0.4022
Length~ Trophic.Niche: Flight.Performance	0.6779119	0.005954	0.0004962	0.04138	0.6808	−0.7465	0.7708
Length~ Primary.Lifestyle: Flight.Style	0.7554063	0.007685	0.0005911	0.05104	0.7386	−0.6286	0.7374
Relative length~ Habitat	0.9289484	0.0003975	4.9684e-05	0.04226	0.7171	−0.37406	0.6516
Relative length ~ Phy.group	0.8517113	0.0002509	4.1814e-05	0.02923	0.6625	−0.41199	0.6614
Relative length ~ Trophic.Level	0.8960627	0.0000910	3.0324e-05	0.0101	0.4591	−0.39659	0.6635
Relative length ~ Trophic.Niche	0.920718	0.0007242	8.0468e-05	0.0779	0.5386	0.5386	0.294
Relative length ~ Primary.Lifestyle	0.8609177	0.0003570	8.9241e-05	0.0412	1.4397	0.75544	0.2279

Note: Numbers in bold indicate statistical significance ($p < 0.05$).

2.3. Uncinate process shape

We captured the morphology of the uncinate process from each species through two approaches: 1) measurement of length and orientation and 2) landmark-based geometric morphometric analysis. The length of the uncinate process was measured from tip to base, while the intercostal angle was measured between the long axis of the distal part of the uncinate process, and the line of attachment between the uncinate process and the rib. For geometric morphometric analysis, all figures were converted into TPS files in the software tpsUtil, ver. 1.83 (Rohlf, 2023) and landmarking was then performed in the software tpsDig 2 ver. 2.31 (Rohlf, 2017). Two point-landmarks and one curve semilandmark (20 semilandmarks) were used to quantify variance in uncinate process shape. The landmark configurations were subjected to a Procrustes analysis to remove geometric information related to scaling, translation and rotation, using the 'gpagen' function of the *geomorph* 4.04 R package (Adams et al., 2022) with the Minimum Bending Energy sliding method (Bookstein, 1996, 1997).

2.4. Principal components analysis

Shape data (Procrustes coordinates) were subjected to a principal components analysis (PCA) to visualise uncinate process morphological variance using the 'gm.prcomp' function in *geomorph*. We first ran an analysis of the dataset with extant birds to investigate the relationships between shape information and known autecological parameters of the various species. Then, we reran the analysis with the dataset including non-neornithine Mesozoic avian species to compare shape variance between neornithines and non-neornithines. Shape changes in the uncinate process associated with each of the first four major axes of total shape variance (PC1-PC4) were visualised by plotting the uncinate process outlines implied by scores of 0.1 and 0.9 for each PC axis. Plotting was performed by means of thin-plate spline deformation (Bookstein & Green, 1993) using 'shape.predictor' from *geomorph*, and landmark constellations were coloured based on per-landmark-variances using the 'hot.dots' function (freely available following this link: https://zenodo.org/record/3929193).

2.5. Multivariate statistics

Phylogenetic generalised least-squares (PGLS) linear models were conducted using the 'pgls' function in *casper* package (Freckleton et al., 2002) to estimate whether uncinate process length (log10 absolute length) is isometrically related to body mass (log10 body mass). Also, the 'procD.pgls' function in *geomorph* would be conducted in order to estimate the main effects and interactions of uncinate process size (log10 centroid size), body mass (log10 body mass), phylogenetic group, and all the autecological variables considered in this study, in relation to shape variance. Because procD.pgls assumes a single-rate Brownian motion model of evolution (Adams et al., 2022), we re-scaled the branches of the calibrated phylogenetic tree to adjust the phylogenetic variation-covariation matrix to a Brownian motion process (e.g. Fabbri et al., 2021; Kuo et al., 2024). In order to do so, we initially used the 'phylosig' function of the package *phytools* v.1.03 (Revell, 2012) to run each PGLS regression, to estimate the value of Pagel's lambda in the resulting residuals. Next, we applied this value of Pagel's lambda to rescale our phylogeny using the function 'rescale' in the package *geiger* v. 2.0.10 (Pennell et al., 2014). Then, each PGLS regression was conducted a second time.

3. Results

3.1. Uncinate process length, species autecology, avian phylogeny and body mass

The uncinate process lengths of the extant birds in our sample ranged from 1.89 mm in the Puerto Rican tody (*Todus mexicanus*) to 48.66 mm in the Emperor penguin (*Aptenodytes forsteri*) (Figure 3(A)). Our PGLS regressions show that uncinate process length is isometrically related to body mass. Furthermore, four ecological parameters (primary habitat, trophic niche, primary lifestyle, flight performance) exhibit

significant correlations with uncinate process length, with R^2 values of 13%, 22%, 11%, and 31%, respectively (Table 1). None of the ecological attributes shows a significant relationship to relative length, i.e. uncinate process length corrected for body mass (Table 1).

Strisoran uncinate processes are generally short, while palaeognathous and aequornithine uncinate processes are longer. The strongest correlation found across Neornithes is between uncinate process length and body mass, with R^2 of nearly 0.8 (Table 1). The length of the uncinate process could be largely explained by body mass in most birds, with the notable exception of the Alagoas curassow in which the uncinate process is proportionally short (Figure 3(A)).

Variance partitioning shows that body mass was the primary independent predictor of uncinate process length, explaining 31.1% of variation uniquely (Table S3 and Figure S3). In contrast, trophic niche and flight performance contributed only minor unique effects, with 0.4% and 1.5%, respectively. A substantial proportion of variation was jointly explained by multiple predictors, indicating strong covariation among body size and these ecological traits. Overall, 81.6% of the variation was explained by the combined model (uncinate process length – body mass, trophic niche, flight performance).

When Mesozoic groups are incorporated into the analysis, a similar relationship between body mass and uncinate process length is recovered (Figure 3(C)). The enantiornithine STM11-128 has an uncinate process length of 4.75 mm, and an estimated body mass of ~171 g (Field et al., 2013). Its uncinate process length is similar to those of extant *Upupa epops* (4.52 mm), *Podargus strigoides* (4.81 mm), *Cyrtonyx montezumae* (4.81 mm), *Scopus umbrette* (4.84 mm), and *Tockus erythrorhynchus* (4.85 mm), which range in body mass from 47.45 g to 472 g. Among these extant species, *Cyrtonyx montezumae* has the closest body mass (185.38 g) to the enantiornithine STM11-128.

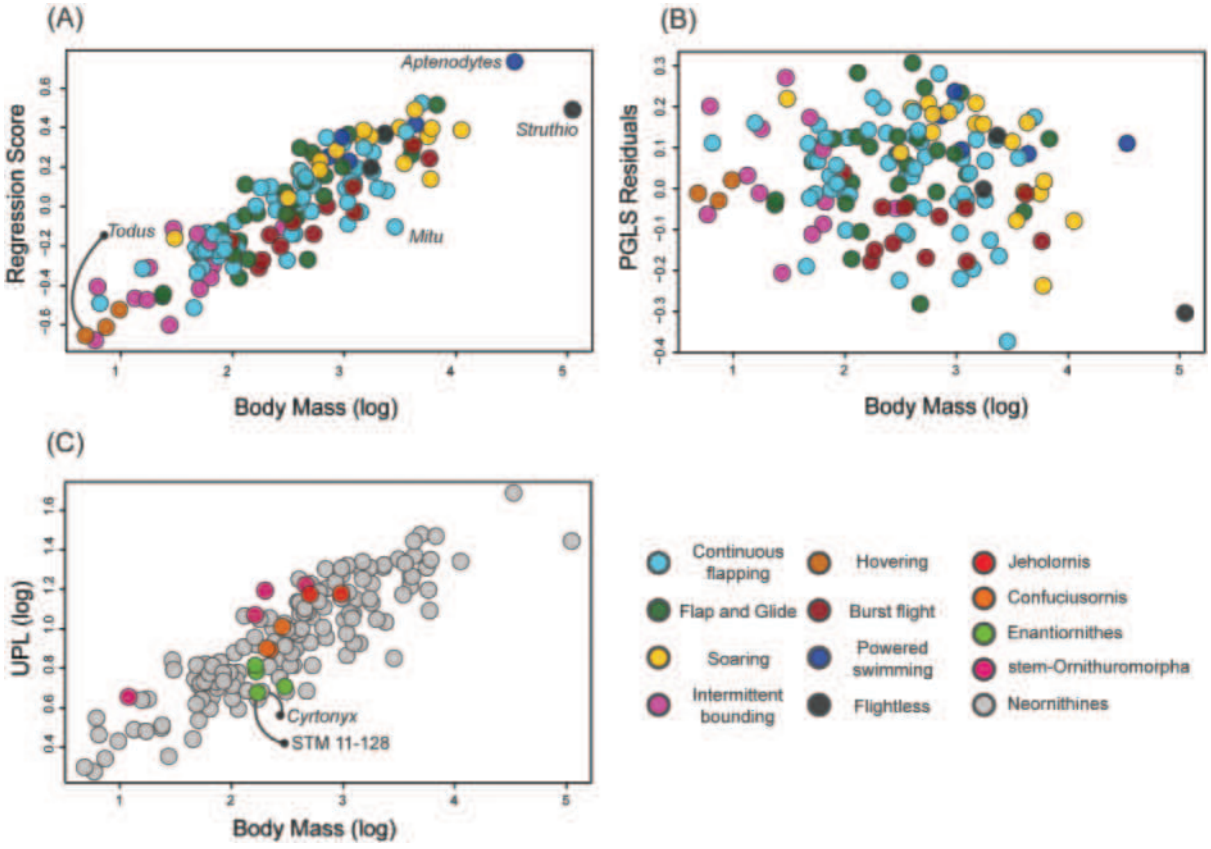

Figure 3. Relationships between uncinate process length and body mass in Neornithes (A), and between phylogenetic generalised least squares (PGLS) residuals scores and body mass in Neornithes (B). Relationship between uncinate process length and body mass in birds (C). Bird species are coloured according to flight performance in A–B (see methods) and according to phylogenetic placement in C. Uncinate process length (mm) and body mass (g) are logged.

3.2. Main patterns of uncinate process variation in Aves

Approximately, 82% of the variance in uncinate process shape among extant birds is captured by PCs 1–3 (PC1 52.8%, PC2 16.7%, PC3 12.2%) (Fig. S5).

PC1 represents the relative width of the base of the uncinate process: in PC1 positive space, the uncinate process tip is relatively blunt with a wide base, as seen in the Hoatzin and Four-banded sandgrouse (*Pterocles quadricinctus*) (Figure 4(A)). In PC1 negative space, the uncinate process is substantially more slender and elongate with a narrow base, as seen in the Eastern screech owl (*Megascops asio*) and Razorbill (*Alca torda*) (Figure 4(A)). PC2 captures changes in the width of the uncinate process. Avian species with a wide uncinate process (e.g. Montezuma quail [*Cyrtonyx montezumae*] and Ostrich [*Struthio camelus*]) occupy PC2 positive space, while avian taxa with thin uncinate processes (e.g. White-necked jacobin [*Florisuga mellivora*] and Red-shouldered hawk [*Buteo lineatus*]) occupy PC2 negative space (Figure 4(A)). PC3 captures the presence of a ventral expansion on the uncinate process, forming a square-like base. In the positive region, the uncinate process base lacks the dorsal expansion, as seen in the Secretarybird (*Sagittarius serpentarius*) and Four-banded sandgrouse (Figure 4(B)). In PC3 negative space, the base of the uncinate process shows a significant expansion. In some species (e.g. Montezuma quail and Moluccan eclectus [*Eclectus roratus*]), this expansion ventrally or ventrocaudally forms another 'process' (*angulus basalaris processi*; Livezey & Zusi, 2007), producing a distinct shape that deviates from that of a typical avian uncinate process (Figure 4(B)). PC4 indicates the direction of the uncinate process tip. In PC4 positive space, the uncinate process tip points more dorsally, as seen in the Montezuma quail and Secretarybird. In PC4 negative space, the tip of the uncinate process points more dorsocaudally (e.g. Hoatzin and Alagoas curassow) (Fig. S6).

When Mesozoic birds are incorporated into the analysis (Figure 5(A,B)), most variation in uncinate process shape is still captured by the first four PC axes (88.36% in total; PC1: 52.78%; PC2: 17.03%; PC3: 11.53%; and PC4: 7.02%), and each PC axis captures approximately the same type of morphological variation as in the analysis including modern taxa only (Fig. S7). The occupancy of morphospace of Mesozoic birds is apparently smaller than that of extant birds. The uncinate process of the indeterminant enantiornithine (STM11-128) is morphologically similar to those of the Torrent duck (*Merganetta armata*), Cuckoo (*Coccyzus americanus* and *Coccyzus erythropthalmus*) and Cinereous tinamou (*Crypturellus cinereus*) based on Procrustes distances. The uncinate processes of the Torrent duck, Yellow-billed cuckoo and Cinereous tinamou all have a square-like expanded base, similar to that of STM11-128. However, the width and orientation of the uncinate process vary slightly among these different species. For instance, the uncinate process is much thicker in the Torrent duck and Cinereous tinamou than in STM11-128. The orientation of the tip is more caudal in the Yellow-billed cuckoo, and more dorsal in the enantiornithine STM11-128.

In contrast to STM11-128, most non-ornithurine birds plot in PC1 negative space, reflecting their more elongate and slender uncinate process morphology (e.g. *Jeholornis* [STM2-7 and STM2-10], *Hongshanornis longicresta* [DNHM 2946] and *Yixianornis grabaui* [IVPP V13631]). Although Mesozoic avians display no clear distribution patterns along PC2, PC3 or PC4, STM11-128 exhibits more extreme PC3 and PC4 values than any other non-neornithine Mesozoic bird (Figure 5(B) & S6).

3.3. Uncinate process shape, species autecology, avian phylogeny, allometry, and body mass

In contrast to the results based on uncinate process length, our PGLS linear models show that most ecological factors of interest (i.e. trophic level, trophic niche and flight performance) lack any significant correlation with uncinate process shape (Table 2). However, habitat and primary lifestyle slightly correlate with uncinate process shape, with respective R^2 values of 10% and 5% (Table 2). These low R^2 values indicate that none of the explored ecological factors strongly explain the observed variation in uncinate process shape. Similarly, neither avian phylogeny nor allometry explains the observed shape variation (Table 2). Body mass correlates weakly with uncinate process shape but only explains 3.4% of the total shape variance (Table 2). When running variation portioning, none of these ecological factors significantly explained the morphological variance of the uncinate process (Table S4 and Figure S4).

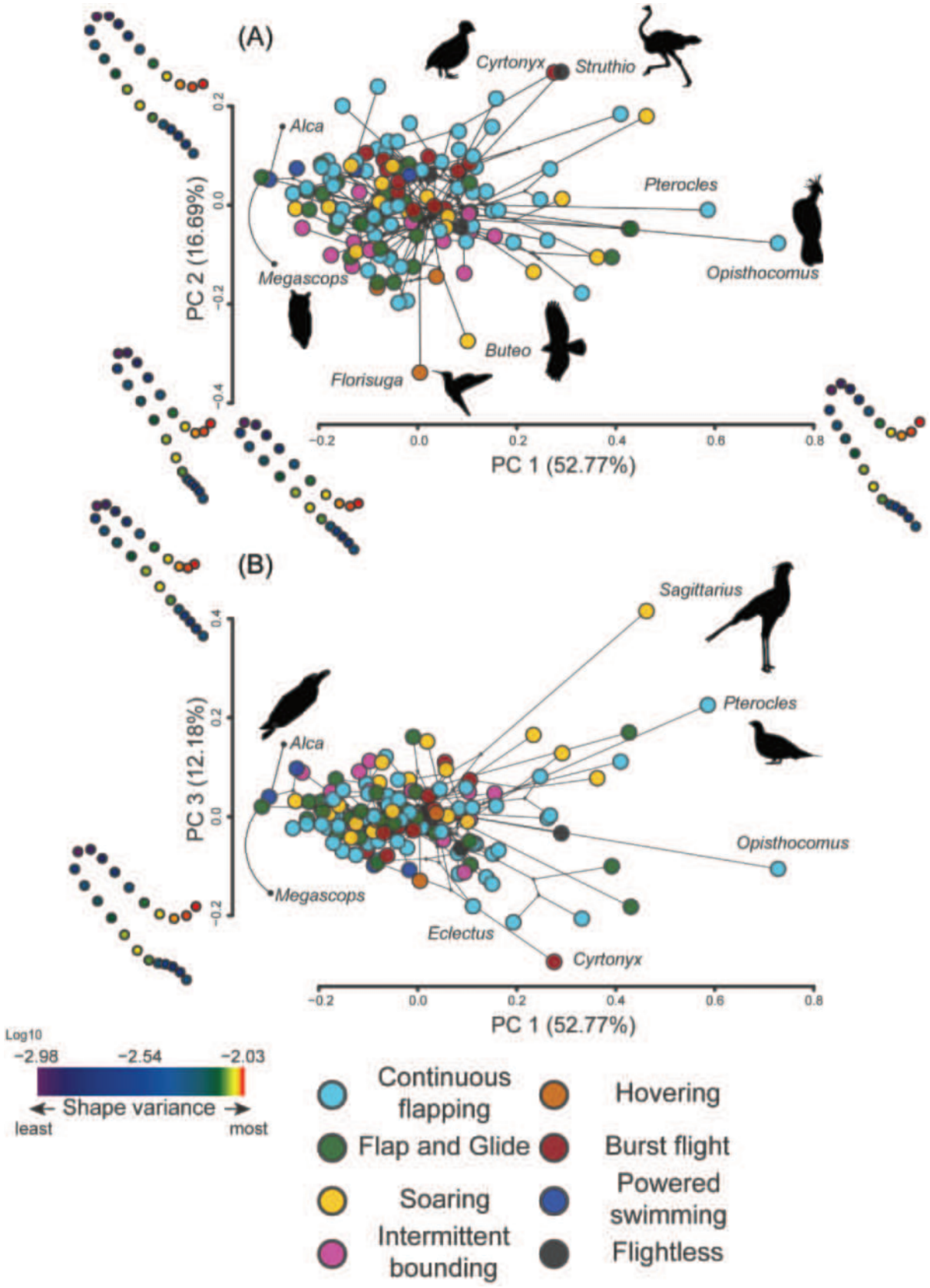

Figure 4. Macroevolutionary patterns of uncinate process shape variation and flight performance in Neornithes. Phylomorphospace defined by the first three axes of uncinate process shape variation. (A) PC1-PC2 and (B) PC1-PC3. Uncinate process models are shown in lateral view and represent 0.9 quantiles of shape variance along PC2 and PC3 (top) in (A) and (B), respectively; 0.1 quantiles of shape variance along PC2 and PC3 (bottom) in (A) and (B), respectively; 0.9 quantiles of shape variance along PC1 (right) in (A) and 0.1 quantiles of shape variance along PC1 (left) in (A). Landmarks and semilandmarks on the uncinate process models are coloured according to log10-transformed per-landmark Procrustes variance. Bird species are labelled by flight style (see material and methods). Silhouettes (1) based on Prof Daniel Field flicker photos or (2) from PhyloPic.Org.

Table 2. Summary of the PGLS liner models for uncinate process shape in Neornithes (n = 139) as a function of ecology information (body mass, primary habitat, trophic level, trophic niche, primary lifestyle, and flight performance), phylogenetic group, and its interaction. Numbers in bold indicate statistical significance ($p < 0.05$).

ANOVA Syntax	λ	SS	MS	R^2	F	Z	P
Shape~Size	0.8673045	0.002285	0.0022846	0.01528	2.1252	1.4946	0.0683
Shape~Uncinate process length	0.8712973	0.001335	0.0013347	0.00887	1.2266	0.63193	0.263
Shape~Body Mass	**0.8557003**	**0.004913**	**0.0049125**	**0.03337**	**4.7292**	**2.7569**	**0.0022**
Shape~Habitat	**0.9092763**	**0.015948**	**0.0019935**	**0.09979**	**1.8013**	**2.1046**	**0.0178**
Shape~Phy.group	0.8316863	0.006395	0.0010659	0.04476	1.0308	0.27759	0.3926
Shape~Trophic.Level	0.866855	0.006009	0.0020029	0.0402	1.8849	1.4692	0.066
Shape~ Trophic.Niche	0.8585381	0.01022	0.0011356	0.06916	1.0649	0.3765	0.3492
Shape~Primary.Lifestyle	**0.8794894**	**0.008082**	**0.0020205**	**0.05309**	**1.8784**	**1.8942**	**0.0276**
Shape~ Flight.Performance	0.8833284	0.009042	0.0012917	0.05906	1.1746	0.65938	0.2518
Shape~Body Mass: Habitat	0.8490835	0.011515	0.0014394	0.07889	1.5193	1.4996	0.0655
Shape~Body Mass: Primary.Lifestyle	0.8959777	0.003737	0.00093417	0.02392	0.8535	−0.24113	0.5951
Shape~Habitat: Primary.Lifestyle	**0.949282**	**0.026910**	**0.0016819**	**0.15479**	**1.5595**	**1.8397**	**0.0328**

4. Discussion

4.1. Uncinate process length, shape and ecological information

Avian uncinate processes are bony projections attached to the dorsal ribs. Given the fact that muscles attached to the uncinate process play important roles in the respiratory system and flight performance, the shape of the uncinate process is likely driven by the ecological attributes. However, according to our PGLS regressions, the shape of the uncinate process is uncorrelated with some of the ecological parameters explored here (e.g. trophic level, trophic niche, flight performance) and only weakly correlated with others (e.g. habitat and primary lifestyle), indicating that uncinate process shape is not strongly driven by any of the ecological factors examined herein. Perhaps other ecological factors, such as breathing and/or metabolic rates, might be strongly connected to the morphological variance of the uncinate processes. However, the data necessary to explore these factors are not available for a wide range of modern species. In addition, to understand the functional importance of uncinate processes, it might be useful to incorporate associated components of the skeleton, such as the sternum (Lowi-Merri et al., 2021, 2023; Widrig et al., 2025) and pectoral girdle to more comprehensively examine the relationships between shape variance and various ecological parameters.

In contrast to shape, uncinate process length shows stronger interactions between body mass, trophic niche, habitat, primary lifestyle, and flight performance. For example, uncinate process length is strongly correlated with body mass, with R^2 values of 0.79. Tickle et al. (2009) obtained a similar result despite using different statistical methodologies and a smaller dataset. Uncinate process length is also weakly related to trophic niche, with R^2 values of 0.21. Scavengers and vertivores have longer uncinate processes, while invertivores and nectarivores have shorter ones. The lack of correlation between autecology and uncinate process shape suggests that the latter has little functional importance. This indicates that the rectangular shape of the uncinate process base observed in some modern birds (e.g. Torrent duck and Yellow-billed cuckoo and Cinereous tinamou) and extinct avians (the enantiornithine STM11-128 and the ornithuromorph *Chaoyangia beishanensis*) likely does not provide extra muscle attachment surface for external oblique muscles, which would allow them to exert more force as drivers of respiratory movements. Instead, these results indicate the length of the uncinate process plays a key role in avian respiration and locomotion. Longer uncinate processes increase the ability of the appendicocostalis and external oblique muscles to contribute mechanically to active locomotion and respiration, by providing either additional area for muscle attachment or longer lever arms. Birds which engage in energy-intensive movements (e.g. continuous flapping) should require commensurately high oxygen intake (Bishop & Butler, 2015), and their uncinate processes would therefore be expected to be longer per unit body mass than those of soaring or flightless birds which consume less energy. However, in our PGLS results, the residuals of the linear model (uncinate process length ~ body mass) do not correspond to flight performance (Figure 3(B)). This shows that, when phylogeny is accounted for, uncinate process length does not exhibit a pattern relating body mass and flight performance, indicating that within each flight performance category uncinate process length and body mass are not strongly associated. Thus, our PGLS residuals indicate that, although uncinate process length is related to flight performance, birds with different flight performance do not exhibit significantly different associations between uncinate process length and body mass. This result is contrary to the findings of Tickle et al. (2009), who explored only three performance categories (divers, non-specialists, and walkers).

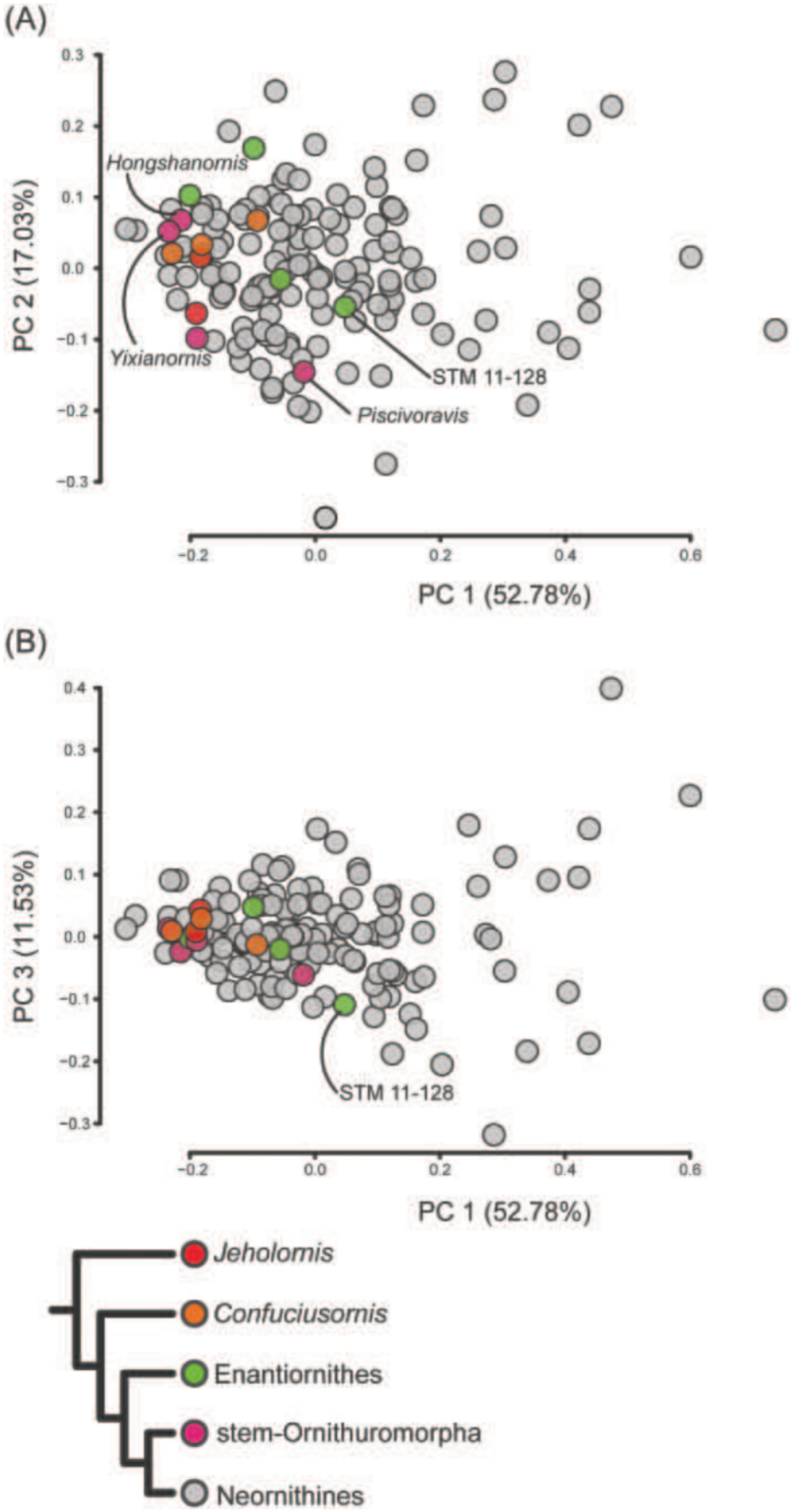

Figure 5. Macroevolutionary patterns of uncinate process shape variation and phylogenetic clades in birds. (A) PC1-PC2 and (B) PC1-PC3. Bird species are coloured according to their phylogenetic positions.

Notably, when Mesozoic avian clades are incorporated into our analyses, uncinate process length also exhibits a strong relationship with body mass, following a pattern similar to that seen in extant avian groups (Figure 3(C)). This indicates that a consistent relationship between uncinate process length and body mass can be traced back to the Early Cretaceous, having been present in *Jeholornis* and basal Pygostylia. Given the correlation between resting metabolic rate and uncinate process length in extant birds (Tickle et al., 2009), uncinate process length in extinct birds might provide some tentative information regarding their metabolic rates. For example, based on body mass and uncinate process length, the metabolic rate of the enantiornithine STM11-128 is estimated to be close to that of a small phasianid, such as Montezuma quail. However, additional research is required to determine when the modern relationship between metabolism and uncinate length evolved, and environmental parameters such as atmospheric oxygen concentration (Mills et al., 2016) would also have to be considered.

4.2. Evolutionary history of the avian uncinate process

During the evolution of the avian uncinate process, this structure gradually diversified from an elongate and slender morphology, as seen in most non-neornithine Mesozoic avian clades, to the highly disparate range of morphologies found in extant birds. Cartilaginous uncinate processes were plesiomorphic for Dinosauria, and the ossified uncinate processes present in most extant avian clades evolved in Maniraptoriformes (Wang et al., 2023). However, the lack of preserved uncinate processes in *Archaeopteryx*, which is known from several well-preserved specimens, suggests that these structures either were cartilaginous (Fig. 21 of Rauhut et al., 2018; Figure 1 of O'Connor et al., 2025), developed late in ontogeny, or potentially were even absent. In *Jeholornis*, the uncinate processes are elongate and unfused, forming an acute angle with the ribs (angle with the rib shaft) (28°–37°) so that they point more dorsally than those of most other Mesozoic birds. In *Confuciusornis*, the uncinate processes are relatively short with blunt tips, and the intercostal angle is much larger (49.7°–55.8°) than in *Jeholornis*.

In Enantiornithes, the morphology of the uncinate process varies in different species: *Parapengornis eurycaudatus* (IVPP V18687) and *Monoenantiornis sihedangia* (IVPP V20289) both exhibit elongate processes with a large intercostal angle (58° and 51°, respectively). The enantiornithine STM29-8 and *Protopteryx fengningensis* (BMNHC Ph 1060a; Figure 6(a) of Chiappe et al., 2020) show uncinate processes similar to those of *Parapengornis* and *Monoenantiornis*, but more dorsally oriented (37° and 32°, respectively). The uncinate processes of *Longipteryx chaoyangensis* (IVPP V12325; Figure 2(e) of Zhang et al., 2001) appear to be narrow with broad bases and blunt tips, pointing relatively caudally (67°). In contrast, the enantiornithine STM11-128 possesses uncinate processes that exhibit two completely different shapes: elongate uncinate processes with fan-like bases and large angles (Figure 2(C)), and processes with a rectangular base and significantly acute intercostal angle (20°) (Figure 2(D)). The latter is unusual among Mesozoic birds, as reflected in its PC 1 positive scores and PC 3 negative scores (Figure 4(B)). This morphology is only otherwise found in the ornithuromorph *Chaoyangia beishanensis*, in which the second of the two preserved uncinate processes has an expanded square-shaped base (IVPP V9934, O'Connor & Zhou, 2013), and in Neornithes. Phylogenetic tree illustrating the evolutionary history of uncinate process morphology in Aves from Jurassic to recent. The diagram includes labeled branches for several important extinct species, such as Archaeopteryx, Jeholornis, Confuciusornis and Enantiornithes.

In non-neornithine Ornithuromorpha, such as *Gansus yumenensis* (Figure 4(B) of Wang et al., 2016), the uncinate processes generally remain simple and elongate as in most non-neornithine birds. However, these processes show a contrasting condition in *Chaoyangia* and *Zhongjianornis yangi* (Zhou & Li, 2010), with the uncinate processes of *Chaoyangia* having rectangular bases similar to those seen in STM11-128, and those of *Zhongjianornis* being relatively short and robust (Figure 4(a) of Zhou & Li, 2010). Most non-neornithine ornithuromorph uncinate processes show an acute intercostal angle, as seen in *Chaoyangia* (52.2°), *Hongshanornis longicresta* (69.1°), and *Yixianornis grabaui* (64.1°). However, the intercostal angle in *Piscivoravis lii* (IVPP V17078; Songlingornithidae) is significantly lower (35.8°) (Figure 6(B) of Chiappe et al., 2014), as shown in the PC1 and PC2 negative scores obtained for this taxon (Figure 5(A)). Intriguingly, uncinate processes have not been found in *Ichthyornis*, although whether they were completely absent, unossified, or simply not fused to the ribs and lost during preservation cannot be determined (Benito et al., 2022).

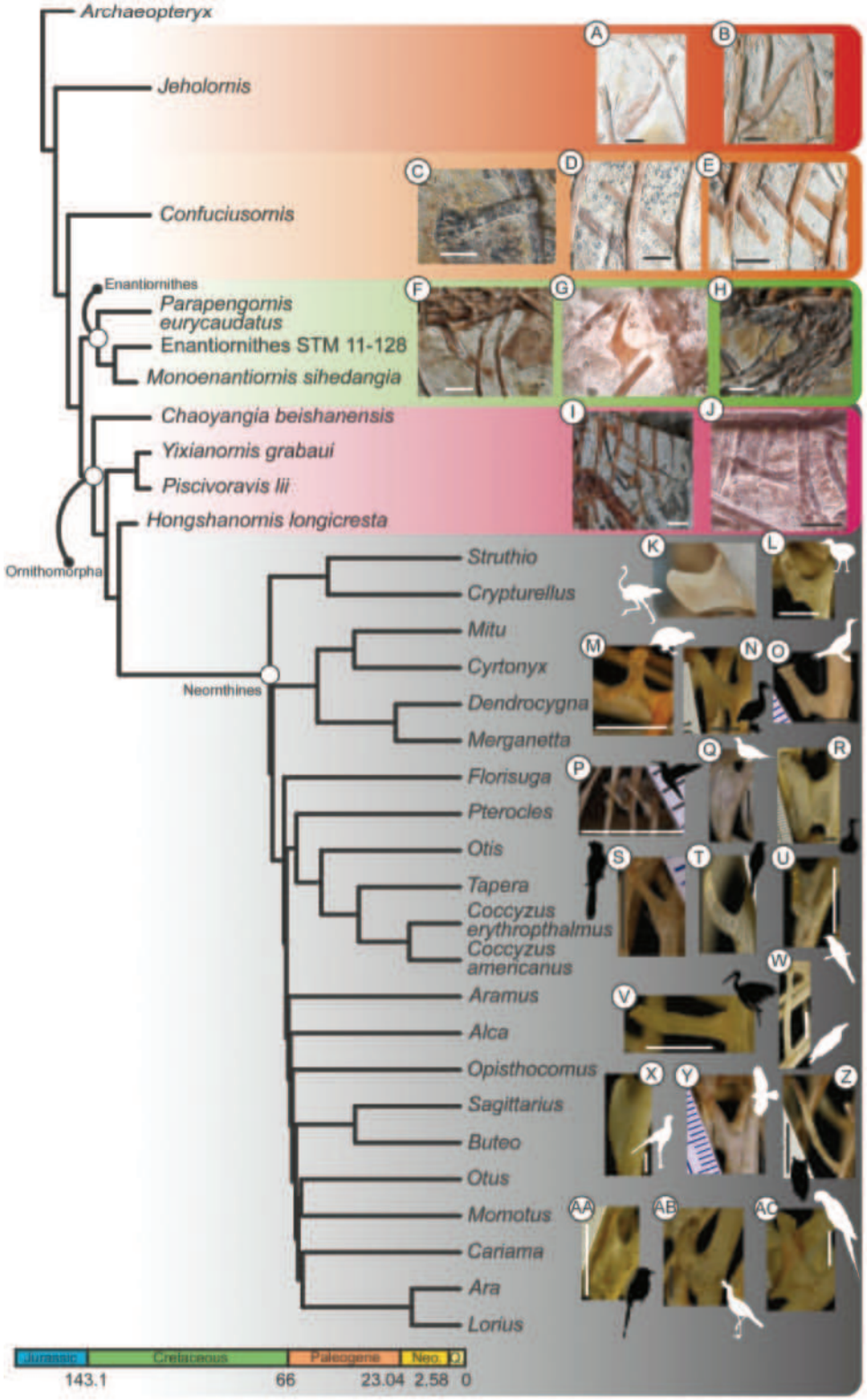

Figure 6. Evolutionary history of uncinate process morphology in Aves. Scale bar: 5 mm. A: *Jeholornis* STM 2–10; B: *Jeholornis* STM 2–7; C: *Confuciusornis* STM 13–35; D: *Confuciusornis* STM 13–170; E: *Confuciusornis* STM 13–44; F: *Parapengornis eurycaudatus* IVPP V18687; G: Enantiornithes STM 11–128; H: *Monoenantiornis sihedangia*; I: *Chaoyangia beishanensis* IVPP V9934; J: *Hongshanornis longicresta* IVPP V2946; K: *Struthio camelus* FMNH uncatalogued; L: *Crypturellus cinereus* FMNH 25,575; M: *Cyrtonyx montezumae* FMNH 106,618; N: *Dendrocygna arborea* FMNH 347,525; O: *Merganetta armata* FMNH 338,969; P: *Florisuga mellivora* FMNH 320,763; Q: *Pterocles quadricinctus* FMNH 319,937; R: *Otis tarda* FMNH 23,514; S: *Tapera naevia* FMNH 376,499; T: *Coccyzus erythropthalmus* FMNH 446,505; U: *Coccyzus americanus* FMNH 526,707; V: *Aramus guarauna* FMNH 368,707; W: *Alca torda* FMNH 432,659; X: *Sagittarius serpentarius* FMNH 105,608; Y: *Buteo lineatus* FMNH 375,999; Z: *Otus asio* FMNH 520,119; AA: *Momotus momota* FMNH 320,994; AB: *Cariama cristata* FMNH 105,635; AC: *Eclectus roratus* FMNH 104,814. Silhouettes (1) based on Prof Daniel Field flicker photos or (2) from PhyloPic.Org.

In Neornithes, the uncinate processes are fully articulated with the caudal margins of the ribs through either complete fusion (Figure 1(A)) or distinct sutures (Figure 1(B)). The morphological variance of neornithine uncinate processes is significantly higher than that of Mesozoic birds, although sampling within the latter set of taxa is extremely limited by poor preservation of the processes (Figures 4(B,D)). Among living birds, the uncinate processes often exhibit the typical elongated outline (Figure 1(A)) but may also be robust and short with a triangular outline as in the Alagoas curassow (Figure 1(B)) and/or weakly developed as in the Hoatzin and Secretarybird (Figures 1(C) and 6(X)). Ventrally expanded rectangular bases similar to those seen in the enantiornithine STM11-128 and *Chaoyangia* occur in several different neornithines, including the Yellow-billed Cuckoo (Figure 6U), Amazonian motmot (*Momotus momota*) (Figure 6(AA)), and Blue-and-yellow macaw. In some extant taxa, the bases of the uncinate processes are significantly expanded to form accessory branches, as observed in the Montezuma quail (Figure 6(M)), West Indian whistling duck (*Dendrocygna arborea*) (Figure 6(N)), Moluccan eclectus, and Great bustard (*Otis tarda*) (Figure 6(R)). The intercostal angle between the uncinate process tip and the rib is typically between 30° and 50° among Neornithes, suggesting that the uncinate process tip generally points caudodorsally. However, the uncinate process in the Limpkin (*Aramus guarana*) points caudally (85.3°) (Figure 6V), while that of the Red-legged Seriema (*Cariama cristata*) points dorsally (5.3°) (Figure 6(AB)). Finally, an accessory pneumatic foramen perforates the base of the uncinate process in some taxa, such as the Blue-and-yellow macaw (Figure 1(D)). The appearance of more complex uncinate processes in the enantiornithine STM11-128, the ornithuromorph *Chaoyangia*, and Neornithes suggests that this shape evolved at least three times independently, and probably many times in the neornithine clades. Although the analyses presented here failed to identify ecological factors that may have driven the evolution of this morphology, the selective pressure involved has evidently acted repeatedly on different groups of birds over at least 120 million years.

5. Conclusion

Avian uncinate processes are thought to contribute strongly to locomotor and respiratory performance, and yet their morphological variation has not been previously investigated. The discovery of an enantiornithine with unusual uncinate morphology (STM11-128), resembling that of some Neornithes, prompted an exploration of uncinate shape evolution across broad swaths of avian evolution. We hypothesised that variation in uncinate process shape might be related to flight performance and other aspects of ecology. However, we found that uncinate process morphology shows a weaker association with ecological categories. In contrast, uncinate process length appears to be significantly associated with flight performance. This might suggest that uncinate process length strongly influences processes such as respiration, which however are unaffected by other aspects of uncinate process shape. Considering the low R^2 values obtained in our analyses, uncinate process shape might correlate most strongly with physiological factors, such as breathing or metabolic rates, as opposed to ecological ones. An alternative possibility is that the morphology of other skeletal elements (e.g. the sternum and pectoral girdle) must be taken into account in future analyses to better understand the significance of the observed shape variation. With respect to differences in uncinate process morphology among avian lineages, non-neornithine clades show lower disparity, consistently having elongate and slender uncinate processes, while uncinate process shape exhibits significantly higher diversity among Neornithes. However, this finding may at least partially reflect preservational bias, as uncinate processes are rarely preserved in the fossil record.

Author contributions

CRediT: **Pei-Chen Kuo:** Conceptualization, Data curation, Formal analysis, Investigation, Methodology, Resources, Visualization, Writing – original draft; **Yan Wang:** Data curation, Investigation; **Alexander D. Clark:** Investigation, Resources, Writing – review & editing; **Corwin Sullivan:** Data curation, Funding acquisition, Writing – review & editing; **Xiaoli Wang:** Data curation, Funding acquisition, Writing – review & editing; **Xiaoting Zheng:** Investigation, Resources; **Jingmai K. O'Connor:** Conceptualization, Investigation, Methodology, Resources, Supervision, Writing – review & editing.

Disclosure statement

No potential conflict of interest was reported by the author(s).

Funding

This study was supported by the National Natural Science Foundation of China (NSFC) [42572027] and the Natural Sciences and Engineering Research Council of Canada [Discovery Grant RGPIN-2023-04916].

ORCID

Pei-Chen Kuo http://orcid.org/0000-0002-5344-6634
Alexander D. Clark http://orcid.org/0000-0003-4310-3408
Corwin Sullivan http://orcid.org/0000-0002-5488-6797
Jingmai K. O'Connor http://orcid.org/0000-0002-3898-8283

Data availability statement

All data are presented in the Supplementary Information. Morphometric landmark coordinates, ecological information, and phylogenetic trees are provided at Zenodo (https://doi.org/10.5281/zenodo.18102802)

References

Adams, D., Collyer, M., Kaliontzopoulou, A., & Baken, E. (2022). *Geomorph: software for geometric morphometric analyses. R package version 4.0.4*. https://cran.r-project.org/package=geomorph

Bapst, D. W. (2012). Paleotree: An R package for paleontological and phylogenetic analyses of evolution. *Methods in Ecology and Evolution*, *3*(5), 803–807. https://doi.org/10.1111/j.2041-210X.2012.00223.x

Baumel, J. J. (1993). *Handbook of avian anatomy: Nomina anatomica avium*. Publications of the Nuttall ornithological club (USA). no. 23.

Benito, J., Chen, A., Wilson, L. E., Bhullar, B. A. S., Burnham, D., & Field, D. J. (2022). Forty new specimens of Ichthyornis provide unprecedented insight into the postcranial morphology of crownward stem group birds. *PeerJ*, *10*, e13919. https://doi.org/10.7717/peerj.13919

Bishop, C. M., & Butler, P. J. (2015). Flight. In C. G. Scanes (Ed.), *Sturkie's avian physiology* (6th ed., pp. 919–974). Academic Press.

Bookstein, F. L. (1996). Combining the tools of geometric morphometrics. *Advances in Morphometrics*, 131–151. https://doi.org/10.1007/978-1-4757-9083-2_12

Bookstein, F. L. (1997). Landmark methods for forms without landmarks: Morphometrics of group differences in outline shape. *Medical Image Analysis*, *1*(3), 225–243. https://doi.org/10.1016/S1361-8415(97)85012-8

Bookstein, F. L., & Green, W. D. (1993, June). Thin-plate spline for deformations with specified derivatives. In *Mathematical methods in medical imaging II* (Vol. 2035. pp. 14–28). SPIE. https://doi.org/10.1117/12.146603

Bretz, W. L., & Schmidt-Nielsen, K. (1972). The movement of gas in the respiratory system of the duck. *Journal of Experimental Biology*, *56*(1), 57–65. https://doi.org/10.1242/jeb.56.1.57

Chiappe, L. M., Di, L., Serrano, F. J., Yuguang, Z., & Meng, Q. (2020). Anatomy and flight performance of the early enantiornithine bird *protopteryx fengningensis*: Information from new specimens of the early Cretaceous huajiying formation of China. *The Anatomical Record*, *303*(4), 716–731. https://doi.org/10.1002/ar.24322

Chiappe, L. M., & Walker, C. A. (2002). *Skeletal morphology and systematics of the Cretaceous. Mesozoic birds: Above the heads of dinosaurs*. University of California Press.

Chiappe, L. M., Zhao, B., O'Connor, J. K., Chunling, G., Wang, X., Habib, M., Marugan-Lobon, J., Meng, Q., & Cheng, X. (2014). A new specimen of the early Cretaceous bird *Hongshanornis longicresta*: Insights into the aerodynamics and diet of a basal ornithuromorph. *PeerJ*, *2*, e234. https://doi.org/10.7717/peerj.234

Clarke, J. A., Zhou, Z., & Zhang, F. (2006). Insight into the evolution of avian flight from a new clade of early Cretaceous ornithurines from China and the morphology of *Yixianornis grabaui*. *Journal of Anatomy*, *208*(3), 287–308. https://doi.org/10.1111/j.1469-7580.2006.00534.x

Codd, J. R. (2010). Uncinate processes in birds: Morphology, physiology and function. *Comparative Biochemistry & Physiology Part A: Molecular & Integrative Physiology*, *156*(3), 303–308. https://doi.org/10.1016/j.cbpa.2009.12.005

Codd, J. R., Boggs, D. F., Perry, S. F., & Carrier, D. R. (2005). Activity of three muscles associated with the uncinate processes of the giant Canada goose Branta canadensis maximus. *Journal of Experimental Biology*, *208*(5), 849–857. https://doi.org/10.1242/jeb.01489

Codd, J. R., Manning, P. L., Norell, M. A., & Perry, S. F. (2008). Avian-like breathing mechanics in maniraptoran dinosaurs. *Proceedings of the Royal Society B: Biological Sciences*, *275*(1631), 157–161. https://doi.org/10.1098/rspb.2007.1233

Fabbri, M., Navalón, G., Mongiardino Koch, N., Hanson, M., Petermann, H., & Bhullar, B. A. (2021). A shift in ontogenetic timing produced the unique sauropod skull. *Evolution*, *75*(4), 819–831. https://doi.org/10.1111/evo.14190

Field, D. J., Lynner, C., Brown, C., & Darroch, S. A. (2013). Skeletal correlates for body mass estimation in modern and fossil flying birds. *PLOS ONE*, *8*(11), e82000. https://doi.org/10.1371/journal.pone.0082000

Freckleton, R. P., Harvey, P. H., & Pagel, M. (2002). Phylogenetic analysis and comparative data: A test and review of evidence. *The American Naturalist*, *160*(6), 712–726. https://doi.org/10.1086/343873

Hu, H., & O'Connor, J. K. (2017). First species of Enantiornithes from Sihedang elucidates skeletal development in early Cretaceous enantiornithines. *Journal of Systematic Palaeontology*, *15*(11), 909–926. https://doi.org/10.1080/14772019.2016.1246111

Hu, H., O'Connor, J. K., & Zhou, Z. (2015). A new species of Pengornithidae (Aves: Enantiornithes) from the lower Cretaceous of China suggests a specialized scansorial habitat previously unknown in early birds. *PLOS ONE*, *10*(6), e0126791. https://doi.org/10.1371/journal.pone.0126791

Kardong, K. V. (1988). Skeletal system: The axial skeleton. In *Vertebrates, comparative anatomy, function, evolution* (pp. 278–279). McGraw-Hill Publishing.

Kimball, R. T., Hosner, P. A., & Braun, E. L. (2021). A phylogenomic supermatrix of Galliformes (landfowl) reveals biased branch lengths. *Molecular Phylogenetics and Evolution*, *158*, 107091. https://doi.org/10.1016/j.ympev.2021.107091

Kirchman, J. J., Rotzel McInerney, N., Giarla, T. C., Olson, S. L., Slikas, E., & Fleischer, R. C. (2021). Phylogeny based on ultra-conserved elements clarifies the evolution of rails and allies (Ralloidea) and is the basis for a revised classification. *Auk*, *138*(4), ukab042. https://doi.org/10.1093/ornithology/ukab042

Kotnour, J., McPeek, S. J., Wedig, H., Dominguez, J., & Wright, N. A. (2022). Relative forelimb–hindlimb investment is associated with flight style, foraging strategy, and nestling period, but not nest type. *Ornithology*, *139*(2), ukab084. https://doi.org/10.1093/ornithology/ukab084

Kuo, P. C., Navalón, G., Benson, R. B., & Field, D. J. (2024). Macroevolutionary drivers of morphological disparity in the avian quadrate. *Proceedings of the Royal Society B: Biological Sciences*, *291*(2017), 20232250. https://doi.org/10.1098/rspb.2023.2250

Lawson, A. B., Hedrick, B. P., Echols, S., & Schachner, E. R. (2021). Anatomy, variation, and asymmetry of the bronchial tree in the African grey parrot (Psittacus erithacus). *Journal of Morphology*, *282*(5), 701–719. https://doi.org/10.1002/jmor.21340

Lerner, H. R., & Mindell, D. P. (2005). Phylogeny of eagles, Old World vultures, and other Accipitridae based on nuclear and mitochondrial DNA. *Molecular Phylogenetics and Evolution*, *37*(2), 327–346. https://doi.org/10.1016/j.ympev.2005.04.010

Liem, K. F., Bernis, W. E., & Walker, W. F., Jr. (2001). The axial skeleton. In *Functional anatomy of the vertebrates: An evolutionary perspective* (3rd ed., pp. 274–276). Harcourt College Publishers.

Liu, G., Zhou, L., Li, B., & Zhang, L. (2014). The complete mitochondrial genome of *Aix galericulata* and *tadorna ferruginea*: Bearings on their phylogenetic position in the Anseriformes. *PLOS ONE*, *9*(11), e109701. https://doi.org/10.1371/journal.pone.0109701

Livezey, B. C., & Zusi, R. L. (2007). Higher-order phylogeny of modern birds (theropoda, Aves: Neornithes) based on comparative anatomy. II. Analysis and discussion. *Zoological Journal of the Linnean Society*, *149*(1), 1–95. https://doi.org/10.1111/j.1096-3642.2006.00293.x

Lowi-Merri, T. M., Benson, R. B., Claramunt, S., & Evans, D. C. (2021). The relationship between sternum variation and mode of locomotion in birds. *BMC Biology*, *19*(1), 1–23. https://doi.org/10.1186/s12915-021-01105-1

Lowi-Merri, T. M., Demuth, O. E., Benito, J., Field, D. J., Benson, R. B., Claramunt, S., & Evans, D. C. (2023). Reconstructing locomotor ecology of extinct avialans: A case study of *ichthyornis* comparing sternum morphology and skeletal proportions. *Proceedings of the Royal Society B: Biological Sciences*, *290*(1994), 20222020. https://doi.org/10.1098/rspb.2022.2020

Maddison, W. P., & Mddison, D. R. (2019). *Mesquite: A modular system for evolutionary analysis. Version 3.61*. See http://www.mesquiteproject.org

McGuire, J. A., Witt, C. C., Remsen, J. V., Corl, A., Rabosky, D. L., Altshuler, D. L., & Dudley, R. (2014). Molecular phylogenetics and the diversification of hummingbirds. *Current Biology*, *24*(8), 910–916. https://doi.org/10.1016/j.cub.2014.03.016

Mills, B. J., Belcher, C. M., Lenton, T. M., & Newton, R. J. (2016). A modeling case for high atmospheric oxygen concentrations during the Mesozoic and Cenozoic. *Geology*, *44*(12), 1023–1026. https://doi.org/10.1130/G38231.1

O'Connor, J. (2022). Enantiornithes. *Current Biology*, *32*(20), R1166–R1172. https://doi.org/10.1016/j.cub.2022.07.074

O'Connor, J., Clark, A., Kuo, P. C., Kiat, Y., Fabbri, M., Shinya, A., Van Beek, C., Lu, J., Wang, M., & Hu, H. (2025). Chicago *Archaeopteryx* informs on the early evolution of the avian bauplan. *Nature*, *641*(8065), 1201–1207. https://doi.org/10.1038/s41586-025-08912-4

O'Connor, J. K., & Zhou, Z. (2013). A redescription of Chaoyangia beishanensis (Aves) and a comprehensive phylogeny of Mesozoic birds. *Journal of Systematic Palaeontology*, *11*(7), 889–906. https://doi.org/10.1080/14772019.2012.690455

Oksanen, J., Simpson, G., Blanchet, F. G., Kindt, R., Legendre, P., Minchin, P., Hara, R., Solymos, P., Stevens, H., Szöcs, E., Wagner, H., Barbour, M., Bedward, M., Bolker, B., Borcard, D., Carvalho, G., Chirico, M., De Cáceres, M., Durand, S., Weedon, J. (2022). *vegan: Community Ecology Package. R package version 2.6-4*. https://CRAN.R-project.org/package=vegan

Oliveros, C. H., Field, D. J., Ksepka, D. T., Barker, F. K., Aleixo, A., Andersen, M. J., Alström, P., Benz, B. W., Braun, E. L., Braun, M. J., Bravo, G. A., Brumfield, R. T., Chesser, R. T., Claramunt, S., Cracraft, J., Cuervo, A. M., Derryberry, E. P., Glenn, T. C., Harvey, M. G., … Moyle, R. G. (2019). Earth history and the passerine superradiation. *Proceedings of the National Academy of Sciences*, *116*(16), 7916–7925. https://doi.org/10.1073/pnas.1813206116

Pennell, M., Eastman, J., Slater, G., Brown, J., Uyeda, J., Fitzjohn, R., Alfaro, M., & Harmon, L. (2014). Geiger v2.0: An expanded suite of methods for fitting macroevolutionary models to phylogenetic trees. *Bioinformatics*, *30*(15), 2216–2218. https://doi.org/10.1093/bioinformatics/btu181

Prum, R. O., Berv, J. S., Dornburg, A., Field, D. J., Townsend, J. P., Lemmon, E. M., & Lemmon, A. R. (2015). A comprehensive phylogeny of birds (Aves) using targeted next-generation DNA sequencing. *Nature*, *526*(7574), 569–573. https://doi.org/10.1038/nature15697

Rauhut, O. W. M., Foth, C., & Tischlinger, H. (2018). The oldest archaeopteryx (Theropoda: Avialiae): A new specimen from the Kimmeridgian/Tithonian boundary of Schamhaupten, Bavaria. *PeerJ*, *6*, e4191. https://doi.org/10.7717/peerj.4191

R Core Team. (2022). *R: A language and environment for statistical computing*. R Foundation for Statistical Computing. https://www.R-project.org/

Revell, L. J. (2012). Phytools: An R package for phylogenetic comparative biology (and other things). *Methods in Ecology and Evolution*, *3*(2), 217–223. https://doi.org/10.1111/j.2041-210X.2011.00169.x

Rohlf, F. J. (2017). *tpsDig2, version 2.31. Stony Brook NY: Department of ecology and evolution*. State University of New York. https://www.sbmorphometrics.org/

Rohlf, F.J. (2023). *tpsUtil, version 1.83*. Department of Ecology and Evolution, State University of New York. https://www.sbmorphometrics.org/

Scheid, P., & Piiper, J. (1972). Cross-current gas exchange in avian lungs: Effects of reversed parabronchial air flow in ducks. *Respiration Physiology*, *16*(3), 304–312. https://doi.org/10.1016/0034-5687(72)90060-6

Sereno, P. C. (1997). The origin and evolution of dinosaurs. *Annual Review of Earth and Planetary Sciences*, *25*(1), 435–489. https://doi.org/10.1146/annurev.earth.25.1.435

Sorensen, M. D., & Payne, R. B. (2005). *A molecular genetic analysis of cuckoo phylogeny*. The cuckoos. Oxford University Press, Oxford.

Tickle, P. G., Ennos, A. R., Lennox, L. E., Perry, S. F., & Codd, J. R. (2007). Functional significance of the uncinate processes in birds. *Journal of Experimental Biology*, *210*(22), 3955–3961. https://doi.org/10.1242/jeb.008953

Tickle, P., Nudds, R., & Codd, J. (2009). Uncinate process length in birds scales with resting metabolic rate. *PLOS ONE*, *4*(5), e5667. https://doi.org/10.1371/journal.pone.0005667

Tobias, J. A., Sheard, C., Pigot, A. L., Devenish, A. J. M., Yang, J., Sayol, F., Neate-Clegg, M. H. C., Alioravainen, N., Weeks, T. L., Barber, R. A., Walkden, P. A., MacGregor, H. E. A., Jones, S. E. I., Vincent, C., Phillips, A. G., Marples, N. M., Montaño-Centellas, F. A., Leandro-Silva, V., Claramunt, S., … Schleuning, M. (2022). AVONET: Morphological, ecological and geographical data for all birds. *Ecology Letters*, *25*(3), 581–597. https://doi.org/10.1111/ele.13898

Vianna, J. A., Fernandes, F. A. N., Frugone, M. J., Figueiró, H. V., Pertierra, L. R., Noll, D., Bi, K., Wang-Claypool, C. Y., Lowther, A., Parker, P., Le Bohec, C., Bonadonna, F., Wienecke, B., Pistorius, P., Steinfurth, A., Burridge, C. P., Dantas, G. P. M., Poulin, E., Simison, W. B., … Nery, M. F. (2020). Genome-wide analyses reveal drivers of penguin diversification. *Proceedings of the National Academy of Sciences*, *117*(36), 22303–22310. https://doi.org/10.1073/pnas.2006659117

Walker, W. F., Jr., & Liem, K. F. (1994). Evolution of the postcranial skeleton. In *Functional anatomy of the vertebrates: An evolutionary perspective* (p. 270). Saunders College Publishing.

Wang, Y., O'Connor, J. K., Li, D., & You, H. (2016). New information on postcranial skeleton of the Early Cretaceous *Gansus yumenensis* (Aves: Ornithuromorpha). *Historical Biology*, *28*(5), 666–679. https://doi.org/10.1080/08912963.2015.1006217

Wang, Y. Y., Claessens, L. P., & Sullivan, C. (2023). Deep reptilian evolutionary roots of a major avian respiratory adaptation. *Communications Biology*, *6*(1), 3. https://doi.org/10.1038/s42003-022-04301-z

Welty, J. C. (1988). Bones and muscle. In L. Baptista (Ed.), *The life of birds* (pp. 59–61). W. B. Saunders and Co.

Widrig, K., Alfieri, F., Kuo, P.-C., James, H. F., & Field, D. J. (2025). Quantitative analysis of stem-palaeognath flight capabilities sheds light on ratite dispersal and flight loss. *Biology Letters*, *21*(9), 20250320. https://doi.org/10.1098/rsbl.2025.0320

Zhang, F., Zhou, Z., Hou, L., & Gu, G. (2001). Early diversification of birds: Evidence from a new opposite bird. *Chinese Science Bulletin*, *46*(11), 945–949. https://doi.org/10.1007/BF02900473

Zhou, S., Zhou, Z., & O'Connor, J. (2014). A new piscivorous ornithuromorph from the Jehol biota. *Historical Biology*, *26*(5), 608–618. https://doi.org/10.1080/08912963.2013.819504

Zhou, Z., & Li, F. Z. Z. (2010). A new lower Cretaceous bird from China and tooth reduction in early avian evolution. *Proceedings of the Royal Society B: Biological Sciences*, *277*(1679), 219–227. https://doi.org/10.1098/rspb.2009.0885